Published in final edited form as:

Sci Transl Med. 2018 September 26; 10(460): . doi:10.1126/scitranslmed.aat7163.

Disrupting the LINC Complex in Smooth Muscle Cells Reduces Aortic Disease in a Mouse Model of HGPS

Paul Kim[1], **Jennings Luu**[1], **Patrick Heizer**[1], **Yiping Tu**[1], **Thomas A. Weston**[1], **Natalie Chen**[1], **Christopher Lim**[1], **Robert L. Li**[1], **Po-Yu Lin**[2], **James C. Y. Dunn**[2], **Didier Hodzic**[3], **Stephen G. Young**[1,4,*], and **Loren G. Fong**[1,*]

[1]Department of Medicine, University of California, Los Angeles, CA 90095, USA.

[2]Department of Surgery, Stanford University School of Medicine, Palo Alto, CA 94305, USA.

[3]Department of Developmental Biology, Washington University School of Medicine, St. Louis, MO 63110, USA.

[4]Department of Human Genetics, University of California, Los Angeles, CA 90095, USA.

Abstract

Hutchinson-Gilford progeria syndrome is a progeroid disorder of children caused by *de novo* mutations in *LMNA* that lead to the synthesis of an internally truncated form of prelamin A (commonly called progerin). The production of progerin causes multiple disease phenotypes, including an unusual vascular phenotype characterized by the loss of smooth muscle cells in the arterial media and fibrosis of the adventitia. In this report, we show that progerin expression, combined with mechanical stress, promotes smooth muscle cell death. Disrupting the LInker of Nucleoskeleton and Cytoskeleton (LINC) complex in smooth muscle cells ameliorates the toxic effects of progerin on smooth muscle cells and limits the accompanying adventitial fibrosis.

Introduction

Hutchinson-Gilford progeria syndrome (HGPS), the classic progeroid disorder of children, elicits multiple disease phenotypes resembling premature aging (1–6). Affected children appear normal at birth but soon manifest failure-to-thrive (gaining ~0.44 kg/yr), hair loss, sclerodermatous skin, joint contractures, and a variety of dental and bone abnormalities. However, certain hallmarks of physiologic aging are absent (*e.g.*, arthritis, cancer, dementia), prompting some to refer to HGPS as a “segmental aging syndrome” (7). Children with HGPS die at a mean age of 14.6 years, generally from occlusive arteriosclerotic disease in the coronary and cerebral arteries (6, 8). The classical form of HGPS is caused by a *de novo* mutation in *LMNA* that results in the synthesis of a mutant form of prelamin A, commonly called progerin (3, 9).

*To whom correspondence should be addressed: Loren G. Fong, Ph.D. or Stephen G. Young, M.D., 695 Charles E. Young Dr. South, Los Angeles, CA 90095. lfong@mednet.ucla.edu, sgyoung@mednet.ucla.edu.

Author contributions: Designing research studies (PK, SGY, LGF), conducting experiments (PK, JL, PH, YT, TAW, CL, NC, RLL, LGF), providing reagents (P-YL, JCYD, DH), and writing the manuscript (PK, SGY, LGF).

Competing interests: The authors declare no competing interests.

LMNA normally yields two alternatively spliced transcripts, one for prelamin A (the precursor to mature lamin A) and the other for lamin C (10). Prelamin A terminates with a carboxyl-terminal *CaaX* motif, which triggers farnesylation of a carboxyl-terminal cysteine, endoproteolytic cleavage of the last three amino acid residues, carboxyl methylation of the newly exposed farnesylcysteine, followed by the release of 15 additional amino acids by ZMPSTE24 (11). The final ZMPSTE24 cleavage step removes the carboxyl-terminal farnesylcysteine methyl ester and releases mature lamin A. The posttranslational processing of prelamin A is thought to aid in the assembly of the nuclear lamina by targeting farnesyl-prelamin A to the inner nuclear membrane. Lamin C is 74 residues shorter than mature lamin A (including 6 unique amino acids at its carboxyl-terminus) and does not undergo any of the aforementioned posttranslational processing steps. Lamins A and C, together with lamins B1 and B2, are the building blocks for the nuclear lamina—a filamentous meshwork lining the inner nuclear membrane (12)—in somatic cells. In interphase cells, the nuclear lamina interacts with nuclear chromatin, proteins of the inner nuclear membrane, nuclear pore complexes, and indirectly to the cytoskeleton *via* the LINC (LInker of the Nucleoskeleton and Cytoskeleton) complex (13). Because of these physical interactions, defects in the nuclear lamina can affect multiple nuclear-related properties (*e.g.*, heterochromatin organization, nuclear membrane integrity, gene expression) (14–20).

The most common mutation underlying HGPS is a point mutation in *LMNA* codon 608 that promotes utilization of an alternative splice-donor site, leading to an in-frame deletion of 50 amino acids and the production of a mutant prelamin A (progerin) (3, 9). The internal deletion does not affect prelamin A's *CaaX* motif but eliminates the upstream ZMPSTE24 cleavage site. Thus, progerin undergoes farnesylation and methylation but does not undergo the final endoproteolytic cleavage step mediated by ZMPSTE24, meaning that the carboxyl terminus of progerin retains its farnesylcysteine methyl ester. Progerin accumulates in the nuclear envelope (16, 21), resulting in misshapen nuclei (3), DNA damage (22, 23), increased sensitivity to mechanical strain (24, 25), and cell senescence (26–28). Inhibiting the farnesylation of progerin with protein farnesyltransferase inhibitors minimizes several of these phenotypes (21, 29–31).

Mice engineered to produce progerin, either globally or in specific tissues, exhibit a variety of disease phenotypes resembling those in children with HGPS (*e.g.*, alopecia, loss of subcutaneous adipose tissue, skeletal abnormalities, retarded growth, shortened lifespan) (32–38). Approximately 15 years ago, Varga *et al.* (39) generated a transgenic mouse with a 164.4-kb BAC clone containing four genes, including *LMNA* (modified to contain the most common HGPS point mutation). The transgenic line did not manifest some of the hallmarks of progeria (*e.g.*, skeletal abnormalities, shortened lifespan), but they developed vascular pathology—loss of smooth muscle cells (SMCs) in the media of the aorta along with fibrosis of the adventitia. The studies were intriguing because they seemed potentially relevant to the vascular disease observed in children with HGPS. Children with HGPS develop atherosclerotic lesions within the arterial intima (8), but SMC loss and adventitial fibrosis have also been observed (8, 40, 41). The cause of SMC loss is unknown but it has been speculated that mechanical stress plays a role (8, 25, 39, 41). Over the past seven years, other groups have observed aortic disease in mouse models of HGPS (35, 38, 42), but there has been little progress in understanding the etiology of the vascular lesions. For example,

given that progerin is expressed in many tissues, it is unclear why the pathology is so obvious in the aorta but seemingly absent in other tissues. Also, why does progerin lead to SMC death, and what causes adventitial fibrosis? Do mechanical forces in large arteries contribute to SMC loss? In the current studies, we investigated those topics using both cell culture and mouse models.

Results

Vascular disease in the aorta of Lmna^{G609G} mice

To investigate the aortic pathology associated with HGPS, we studied a knock-in mouse model (*Lmna*^{G609G}) with a mutant *Lmna* allele harboring the most common point mutation found in children with HGPS (38). Both *Lmna*$^{G609G/+}$ and *Lmna*$^{G609G/G609G}$ mice develop progressive disease phenotypes (*e.g.*, skeletal abnormalities, reduced body weight gain), but disease phenotypes appear at an earlier age and progress more rapidly in *Lmna*$^{G609G/G609G}$ mice (Fig. S1a). Western blotting confirmed the synthesis of progerin (and the absence of prelamin A) in the aorta (Fig. 1a), and hematoxylin and eosin (HNE) staining revealed hallmark vascular phenotypes in the ascending thoracic aorta [loss of smooth muscle cells (SMCs), adventitial thickening, intact endothelium] (Fig. 1b). To quantify the vascular phenotype, the density of SMC nuclei (nuclei per μm^2 media area) and adventitial area as a percentage of total area were measured in 4-month-old *Lmna*$^{G609G/G609G}$ mice. In those mice, the density of SMC nuclei was reduced by >90% in the proximal ascending aorta, and the adventitial area was ~threefold greater than in wild-type mice (Fig. 1c). The vascular phenotype was also observed in other regions of the aorta. Disease was present in the mid-arch, proximal descending aorta, and the lower descending aorta (Fig. 1e and Fig. S1b); the same pathology was observed in the brachiocephalic, right and left common carotid, and left subclavian arteries (Fig. S1c). On H&E staining, the muscle layer of the aorta stained less red (*e.g.*, Fig. 1e), and some SMCs contained vacuoles (Fig. 1f). No disease was detected in wild-type mice (Figs. 1e and Fig. S1b) or *Zmpste24*$^{-/-}$ mice (where there is an accumulation of the farnesylated form of wild-type prelamin A) (Fig. S1d). The onset of aortic disease occurred *after* two months of age [aortas in two-month-old *Lmna*$^{G609G/+}$ and *Lmna*$^{G609G/G609G}$ mice were free of obvious pathology (Fig. S2a)]. We did not observe similar pathology in the parenchyma of other tissues (*e.g.*, kidney, skeletal muscle) (Figs. S2b–c).

Intranuclear vesicles in Lmna^{G609G} aortic smooth muscle cells

Transmission electron microscopy identified two unusual features in *Lmna*^{G609G} aortic SMCs. The first was nuclei containing multiple intranuclear vesicles (Fig. 1g and Figs. S3a–b). The vesicles were bounded by inner and outer nuclear membranes, with heterochromatin lining the inner nuclear membrane, and occasionally containing cytoplasmic material. These structures were not observed in endothelial or adventitial cells (Fig. S3c). The second unusual feature was that some SMCs contained multiple cytoplasmic vesicles (Fig. 1g and Fig. S3b). Most of the vesicles appeared to be surrounded by a single lipid bilayer. We suspect that these represented dying cells with cytoplasmic autolysosomes (43).

Collagen VIII synthesis is activated in the aortic adventitia of Lmna^{G609G} mice

Previous histological studies showed increased collagen in diseased aortas (38, 39). In keeping with those findings, we observed increased collagen content in aortas of *Lmna*$^{G609G/G609G}$ mice, as judged by Verhoeff-Van Gieson (VVG) and Masson's trichrome (MT) staining (Fig. 2a; collagen stains red with the VVG stain and blue with the MT stain). To determine the type of collagen that accumulates in diseased aortas, we analyzed gene expression in different layers of the aorta (adventitia *vs.* the media/intima). The layers were separated by enzymatic digestion (44) and validated by the expression of marker genes (*i.e.*, *Col1a1* for the adventitia; *Acta2* and *Tagln* for the media; and *Pecam1* for endothelial cells; Fig. 2b and Fig. S4e). The expression of *Col1a1*, *Col3a1*, *Col5a1*, and *Col8a1* was increased in the adventitia of *Lmna*$^{G609G/+}$ mice, but the largest increases (relative to wild-type mice) were in the expression of *Col1a1* and *Col8a1* (3.8- and 17.2-fold, respectively). *Col1a1* and *Col8a1* expression were also increased in the aortic media, but the levels of expression were much lower than in the adventitia. Immunofluorescence microscopy confirmed increased amounts of collagen types I and VIII protein in the aortic adventitia of *Lmna*$^{G609G/+}$ mice (Fig. 2c).

Lamin A and progerin are expressed highly in the aorta

The toxicity of progerin is dose-related. In cultured cells, increased amounts of progerin result in more misshapen nuclei, more DNA damage, and more rapid senescence (18, 30). In mouse models, the severity of disease expression correlates with levels of progerin expression (32, 33, 35) (Fig. S1a). Given these observations, we suspected that tissues that express the highest levels of progerin would more likely develop disease. To test this idea, the most straightforward approach would be to measure progerin levels in tissues of *Lmna*^{G609G} mice; however, we were concerned that progerin levels might be influenced by the disease itself (*i.e.*, the emergence of disease might influence progerin levels by affecting *Lmna* splicing, cell viability, or protein turnover). To circumvent this possibility, we first examined lamin A levels in wild-type mice, reasoning that lamin A expression in wild-type mice might correlate with progerin expression in *Lmna*^{G609G} mice. Lamin A levels were measured in the brain (cerebral cortex), liver, kidney, intercapsular brown adipose tissue, gonadal white adipose tissue, gallbladder, quadriceps, heart, skin, femur, and aorta (ascending, descending, and abdominal segments) by western blotting (Fig. 3a). Lamin A levels were normalized to tubulin, lamin C, or lamin B1 (Figs. 3b–d). Lamin A expression in the different tissues was variable, differing as much as ~14-fold when normalized to tubulin. Low expression was found in the brain, liver, and kidney, whereas high expression was observed in the aorta, skin, and bone (Fig. 3b). Of note, the latter tissues are sites of pathology in HGPS, whereas the former tissues are not (4). The tissues with high levels of lamin A (*i.e.*, aorta, skin, bone) also exhibited a high lamin A:lamin C ratio (Fig. 3c).

The brain, a tissue that is spared in HGPS, exhibits low levels of lamin A relative to lamin B1 (37, 45). When we ranked lamin A expression relative to lamin B1 expression, the brain was the lowest and the aorta was the highest (Fig. 3d). The differences in expression were also evident at the transcript level (prelamin A:*Lmnb1*) (Fig. 3e).

Based on the pattern of lamin A expression in wild-type mice, we predicted that we would find high levels of progerin expression in the aorta of mice carrying the *Lmna*^{G609G} allele. Indeed, this was the case; the tissue with the highest levels of progerin in *Lmna*$^{G609G/+}$ mice was the aorta (Figs. S4a–d).

Lamin B1 levels are low in aortic medial SMCs

A puzzling feature of the pathology in mouse models of HGPS is the loss of SMCs in the arterial media and the absence of obvious pathology in endothelial cells of the intima and cells of the adventitia. We hypothesized that the susceptibility of different cells to disease might be due to different levels of lamin A expression. To explore this idea, we separated the media and adventitia layers and measured gene expression. Prelamin A transcript levels were similar in the media and adventitia, but lamin B1 levels were ~3–4-fold higher in the adventitia than in the media (Fig. 3f). The higher lamin B1 expression in the adventitia was confirmed by western blotting (Fig. S4f) and immunofluorescence microscopy (Fig. 3g). The microscopy studies also showed that lamin B1 expression was higher in endothelial cells than in medial SMCs. Thus, SMCs have a far higher lamin A:lamin B1 ratio than endothelial cells and adventitial cells.

The vascular phenotype is more severe at curvatures and branches

Our experience in dissecting aortas from *Lmna*^{G609G} mice suggested that the aortic pathology was not uniformly distributed. To determine the distribution of aortic disease, we sectioned the proximal aorta down the midline and stained for CD31 (an endothelial cell marker) and collagen type VIII (a marker of adventitial fibrosis). In 12-month-old *Lmna*$^{G609G/+}$ mice and 4-month-old *Lmna*$^{G609G/G609G}$ mice, the pathology was more pronounced along the inner curvature of the ascending aorta and at major branch points (especially at the origin of the brachiocephalic artery) (Figs. 4a–c). Quantitative studies in *Lmna*$^{G609G/+}$ (Figs. 4d–e) and *Lmna*$^{G609G/G609G}$ (Figs. S5a–c) mice revealed that there was more adventitial fibrosis and a greater loss of SMCs in the media along the inner curvature of the aorta. Similar changes were noted along the posterior wall of the ascending aorta in mice expressing human progerin but the changes were not quantified (42). Given that our western blot and gene expression studies showed a correlation between high lamin A expression (and low lamin B1 expression) and the extent of aortic pathology, we suspected that we might find distinct patterns of lamin A and lamin B1 expression in the inner and outer curvatures of the aorta. However, this was not the case (Fig. 4f).

Progerin expression induces hallmark HGPS phenotypes in cultured SMCs

The fact that the aortic pathology in the HGPS mice was greater in some locations than in others led us to suspect that local biomechanical forces are relevant to disease pathogenesis. This suspicion was not farfetched; the predilection of specific regions of the mouse aorta to atherosclerotic lesions near curvatures and branch points has been attributed to disturbed blood flow and dynamic changes in shear stress (46, 47). To determine if cells expressing progerin have increased sensitivity to mechanical forces, we developed a model system with cultured cells. Mouse SMCs stably expressing either human prelamin A or human progerin were grown on flexible polydimethylsiloxane (PDMS) membranes and exposed to repetitive biaxial stretch. In these studies, a doxycycline-inducible system was used to achieve a lamin

A:lamin C profile similar to that in medial SMCs *in vivo* (*i.e.*, a lamin A:lamin C ratio of 3–4:1) (Fig. 3c). The expression of mature lamin A and progerin depended on doxycycline concentration in the medium, and the optimal expression levels for lamin A and progerin were achieved at 0.1 and 0.3 μg of doxycycline per ml, respectively (Fig. S6a). The expression of progerin in SMCs resulted in "HGPS phenotypes"—misshapen nuclei (Fig. 5a) and markers of DNA damage [an accumulation of phosphorylated p53(ser15) and H2AXγ] (Fig. 5b). However, the expression of progerin did not increase Sun1 protein levels (48), as determined by western blotting with three different commercial antibodies. The increased DNA damage in progerin-expressing cells could not be attributed to the higher concentration of doxycycline required to induce progerin expression because DNA damage was not observed when wild-type cells were incubated with up to 3 μg of doxycycline per ml (Fig. S6b).

Progerin expression promotes cell death in stretched SMCs

To determine if biomechanical forces could contribute to SMC loss in HGPS mice, cells were cultured on flexible PDMS membranes and exposed to repetitive biaxial stretching (25). After 24 h, ~40% of progerin-expressing SMCs detached from the membrane, as judged by cell protein (Fig. 5c). Collection of the detached cells and staining with trypan blue showed that the cells were non-viable. In contrast, SMCs that expressed wild-type prelamin A were unaffected and remained viable. To assess the effects of stretch before cell death and detachment, the cells were stained with propidium iodide (PI) (25) after stretching for 2 h. PI staining increased to ~12% in progerin-expressing SMCs, whereas it increased to only ~1% in lamin A–expressing cells (Fig. S6c). Similarly, reducing lamin B1 levels increased H2AXγ levels to a larger extent in progerin-expressing SMCs than in prelamin A-expression cells (Fig. S6d). Thus, progerin expression renders SMCs more susceptible to cell death in response to mechanical stress.

Disrupting the LINC complex reduces the toxic effects of progerin in cultured SMCs

The cell nucleus is connected to the cytoskeleton by the LInker of the Nucleoskeleton and Cytoskeleton (LINC) complex (13), and this complex is known to transmit biomechanical forces to the cell nucleus. Two outer nuclear membrane proteins of the complex, Nesprin1 and Nesprin2, are tethered to the cytoskeleton while the KASH domains of Nesprin1 and Nesprin2, located within the perinuclear space, interact with the Sun domains of Sun1 and Sun2. Sun1 and Sun2 traverse the inner nuclear membrane and interact with the nuclear lamina (49). The link between the cytoskeleton and the nuclear lamina can be disrupted by overexpressing the KASH domain of Nesprin2 (KASH2). KASH2 expression occupies the binding sites on the Sun proteins and thereby prevents "Sun–Nesprin" interactions within the perinuclear space (50). We predicted that KASH2 expression would reduce force transmission to the nucleus and limit the death of progerin-expressing cells during repetitive stretching. To test this possibility, we generated stable cell lines expressing either a KASH2–EGFP fusion protein (KASH2) and an inactive KASH2–EGFP mutant (ext-KASH2). Remarkably, KASH2 prevented the nuclear shape abnormalities that appear in progerin-expressing cells (Fig. 5d) and simultaneously reduced markers of DNA damage (Fig. 5e). Of note, these effects were observed in the absence of any effects on progerin (Fig. 5e) or lamin B1 levels (lamin B1:actin ratio in ext-KASH-expressing cells of 0.165 ± 0.05 *vs.* 0.163

± 0.01 in KASH2-expressing cells, respectively; $n = 3$ experiments). When progerin-expressing SMCs were exposed to repetitive stretching, the expression of KASH2 increased cell survival by 71% (Fig. 5f) and reduced PI staining by ~60% (Fig. S6c). These studies demonstrate that KASH2-mediated disruption of force transmission to the cell nucleus limits the toxicity of progerin in cultured SMCs.

Disrupting the LINC complex in aortic SMCs ameliorates SMC loss and adventitial fibrosis

The beneficial effects of KASH2 expression in progerin-expressing SMCs prompted us to test whether KASH2 expression in the SMCs of HGPS mice would ameliorate SMC loss in the medial layer of the aorta. To test this idea, we introduced a *Cre*-conditional KASH2–EGFP transgene (51) into *Lmna*$^{G609G/G609G}$ mice harboring a SMC-specific *Sm22-Cre* transgene (52). We bred three groups of mice: *Lmna*$^{+/+}$KASH2–EGFP^{+}*Sm22-Cre*$^{+}$ (WT); *Lmna*$^{G609G/G609G}$KASH2–EGFP^{+}*Sm22-Cre*$^{-}$ (MUT); and *Lmna*$^{G609G/G609G}$KASH2–EGFP^{+}*Sm22-Cre*$^{+}$ (MUT+KASH2). The specificity of the *Sm22-Cre* transgene was confirmed with mT/mG reporter mice (53). *Sm22-Cre*-mediated recombination occurred only in SMCs in the aortic medial layer, as judged by EGFP fluorescence (Fig. S6e). KASH2 expression in the aorta of *Lmna*^{G609G} mice was confirmed by western blotting and this did not affect progerin levels (Fig. S6f). All mice were collected at 4-months of age, before *Lmna*^{G609G} mice die of progeria disease. Thus, the study design does not permit us to determine the effects of KASH2 expression on mouse survival. However, KASH2 expression did not have negative effects on progeria disease, as judged by reduced survival or lower body weights (Fig. S6g). KASH2 expression in MUT mice improved vascular pathology in the ascending aorta (inner and outer curvatures) and proximal descending thoracic aorta (Fig. 6). In the outer curvature of the ascending aorta (Fig. 6a), the density of SMC nuclei increased to 65% of that in WT mice, and adventitial fibrosis was eliminated (Fig. 6e). In the inner curvature, where the aortic pathology is more severe, the density of SMC nuclei increased ~threefold but only to ~33% of the density observed in the aorta of WT mice. Nevertheless, adventitial fibrosis in the ascending aorta was greatly improved (~60% decrease) (Fig. 6f). In the descending aorta, where disease is less severe, the beneficial effects of KASH2 expression were striking (Fig. 6c). The density of SMC nuclei in the medial layer of MUT+KASH2 aortas was 75% as high as in WT mice, and adventitial fibrosis was eliminated (Fig. 6g). These studies demonstrate that force transmission from the cytoskeleton to the nucleus is a significant factor in promoting SMC loss. Moreover, our results show that improved SMC survival prevents adventitial fibrosis, indicating that adventitial fibrosis in HGPS mice is secondary to the loss of SMCs.

Discussion

The vascular pathology of HGPS has fascinated physicians and biomedical investigators for decades (8, 40, 41). Despite an absence of the typical risk factors for atherosclerosis, children with HGPS succumb to heart attacks or stroke, a consequence of occlusions in the coronary and cerebral arteries (54, 55). The arterial pathology in HGPS must be caused by progerin, but the underlying mechanisms have remained unclear. In the current studies, we investigated the vascular pathology in HGPS mice and developed three insights into pathogenesis. The first relates to why the aorta develops disease while other tissues are

spared. We found that the aorta produces more progerin than any other tissue—more than the skin and bone (two tissues affected by HGPS) and ~15-fold more than in the kidney (an unaffected tissue). Electron micrographs of aortic SMCs of HGPS mice revealed striking abnormalities—intranuclear membrane vesicles and vacuoles in the cytoplasm. The second insight is that mechanical forces influence the distribution of vascular lesions. The vascular disease in HGPS mice is most severe along the inner curvature of the ascending aorta and at arterial branch points, where blood flow is disturbed and biomechanical forces are altered (46, 47). The third insight is that reducing force transmission to the nucleus ameliorates the toxicity of progerin. In cultured SMCs, uncoupling the LINC complex with KASH2 (and thereby blunting force transmission to the cell nucleus) resulted in less DNA damage, fewer nuclear blebs, and reduced cell death. Importantly, the expression of KASH2 in SMCs in HGPS mice markedly reduced SMC loss in the aortic media and reduced adventitial fibrosis.

Both the loss of aortic medial SMCs and the accompanying adventitial fibrosis depend on the dosage of progerin (*i.e.*, the onset of vascular disease is earlier and disease progression is more rapid in homozygous HGPS mice than in heterozygous mice). The fact that disease severity depends on progerin dosage is not particularly surprising, given earlier studies showing that progerin expression levels affect the frequency of misshapen nuclei in cultured fibroblasts (18, 30) and mouse experiments showing that the severity of *nonvascular* disease phenotypes depends on levels of progerin expression (32, 33, 35). Of note, in humans, point mutations that increase progerin expression are associated with more severe disease (56).

Given the link between gene dosage and the severity of disease phenotypes, we suspected that we might encounter higher levels of progerin expression in tissues that are susceptible to disease (*e.g.*, aorta, skin, bone) than in tissues that are spared (*e.g.*, liver, kidney, brain). Indeed, this was the case. Of note, the higher levels of progerin expression in aorta, bone, and skin were not secondary to pathology in those tissues, but due to the intrinsic higher expression of lamin A in those tissues as found in wild-type mice (*i.e.*, highest in skin, bone, and aorta and lowest in liver, kidney, and brain). Interestingly, the aorta was third-highest for lamin A expression in wild-type mice (behind skin and bone) but ranked first for progerin expression in HGPS mice. Those observations raise the possibility that progerin might accumulate in the aorta in HGPS mice, perhaps because of lower levels of turnover.

The distribution of vascular lesions was not uniform in the proximal aorta, suggesting that there are regional influences on lesion formation. The vascular disease was most severe along the inner curvature of the ascending aorta and at branches of the aortic arch—the very same locations where early atherosclerotic lesions develop in models of atherosclerosis. The nonrandom formation of atherosclerotic lesions is thought to be due to differences in flow patterns, where lesion formation coincides with areas of disturbed flow and oscillating low shear stress conditions—namely at bends and branch points (46). The fact that HGPS vascular lesions develop in the same locations suggests that low shear stress contributes to the HGPS vascular phenotype. However, it is noteworthy that SMC loss and adventitial fibrosis also occurs along the outer curvature of the ascending aorta (albeit to a lower extent), where shear stress and circumferential vessel strain are high. Thus, HGPS vascular lesions are not limited to regions of low shear stress and suggest that high vessel strain could also lead to SMC loss. Our *in vitro* mechanical stretch studies, which more closely model

high vessel strain, support this proposal. In our studies, the combination of progerin expression and repetitive cell stretching resulted in greater cell toxicity than progerin expression alone.

Disrupting the LINC complex in SMCs with KASH2 expression ameliorated medial SMC loss and adventitial fibrosis throughout the aorta, but the greatest improvement was in regions with the least severe disease—the outer curvature of the ascending aorta and the descending aorta. In those regions, KASH2 expression in SMCs increased the density of medial SMCs to levels approaching those in wild-type mice. Somewhat less expected was the significant reduction of adventitial fibrosis with KASH2. The *Sm22-Cre* transgene used to activate KASH2 expression is specific for medial SMCs in the aorta; hence, the improvement in adventitial fibrosis cannot be attributed to KASH2 expression in the mesenchymal cells of the adventitia. The simplest explanation is that collagen synthesis in the adventitia is activated in response to medial SMC death and weakening of the medial layer. In support of this idea, we observed an inverse relationship between medial SMC density and collagen type VIII staining in the aortic adventitia. Also, in earlier studies, Turlo *et al.* (57) observed aortic adventitial fibrosis in the setting of a genetic intervention (inactivation of β1-integrin) that caused SMC death in the aortic media.

Nearly 20 years ago, Stehbens *et al.* (41) described SMC loss in the aorta in two autopsy cases of “progeria” (a firm diagnosis of HGPS was not established by genetic testing). In the more severe case, the medial layer of the aorta was nearly devoid of SMCs, and immunohistochemistry studies showed increased expression of collagen types I and III in the aortic intima. More recently, Olive *et al.* (8) examined atherosclerotic lesions in two children with *bona fide* HGPS (where a diagnosis of HGPS was confirmed by genetic testing). They observed loss of vascular SMCs in the aorta of one case, but both cases had adventitial fibrosis. Staining with Picrosirius red revealed increased amounts of collagen I and III in the aorta. In our studies, *Col1a1* and *Col3a1* expression were increased in the aortic adventitia of HGPS mice, but the increase in *Col8a1* expression was the most impressive (17-fold greater than in the aorta of wild-type mice). The expression of collagen type VIII in blood vessels is normally very low, but increased expression has been observed in the setting of vascular injury and atherosclerosis (58, 59). Further studies will be required to determine if increased levels of collagen type VIII also occur in other diseased tissues (*e.g.*, skin, bone).

An intriguing issue is why medial SMCs in HGPS mice die while the endothelial cells in the arterial intima and the mesenchymal cells of the adventitia are viable. We doubt that these differences can be fully explained by differences in progerin expression. We found similar levels of prelamin A transcripts in the media and adventitia of the mouse aorta, and the levels of lamin A protein in the aorta media were only ~twofold higher than in the adventitia. We speculate that the peculiar susceptibility of medial SMCs to cell death could relate to low levels of lamin B1 expression. By immunofluorescence microscopy, lamin B1 expression in medial SMCs is low—far lower than in intimal endothelial cells or adventitial cells. Gene-expression and western blotting studies confirmed those findings. Low levels of lamin B1 expression have been reported to cause stiffer cell nuclei (60) and to induce senescence (61)—similar to phenotypes elicited by progerin. We speculate that increased rigidity of cell nuclei in medial SMCs (where progerin levels are high and lamin B1 levels

are low) renders the nucleus more susceptible to nuclear membrane ruptures (20, 62), which could lead to DNA damage and cell death (63). Additional studies are required to investigate the role of low lamin B1 levels in the increased mechanical sensitivity of SMCs.

The ultrastructural hallmark of aortic medial SMCs in HGPS mice are intranuclear vesicles bounded by a double membrane and surrounded by heterochromatin. We suspect that these intranuclear vesicles, which are absent from intimal endothelial cells and adventitial cells, are the result of tubular invaginations of the nuclear envelope. In support of this idea, we have observed cytoplasmic contents “inside” the intranuclear vesicles. We do not understand the mechanism for the tubular invaginations, but one possibility is that high progerin levels lead to increased nuclear membrane synthesis (64), which in turn results in tubular invaginations. The consequences of deep nuclear membrane invaginations are unknown, but it is easy to imagine that these structures could disrupt chromatin architecture and gene expression. It is also conceivable that the transmission of cytoskeletal forces to intranuclear vesicles would be tangential to the surface of the nucleus (or would occur in multiple directions), increasing the likelihood of nuclear membrane ruptures.

In mouse models of atherosclerosis driven by hyperlipidemia, the atherosclerotic lesions preferentially form at sites of disturbed flow and oscillating shear stress (the inner curvature of the ascending aorta and at branches of the aortic arch) (46). Those sites are identical to sites of vascular pathology in HGPS mice, implying that shear stress is a common factor in the pathogenesis of hyperlipidemia-driven atherosclerosis and the vascular pathology in HGPS. Although atherosclerosis is generally considered to be an intimal disease, the loss of SMCs in the media and the resultant weakening of the aorta could lead indirectly to more atheromas in the intima. Of note, Clarke *et al.* (65) have shown that inducing vascular SMCs apoptosis in *Apoe*$^{-/-}$ mice (a model of atherosclerosis) induces intense intimal inflammation and characteristics of atherosclerotic plaque vulnerability (*i.e.*, thin fibrous cap, inflammatory foci, large necrotic core, cellular debris, depletion of matrix content). Alternatively, it is entirely possible that progerin expression in arterial endothelial cells, accompanied by increased biomechanical forces, leads to more subtle (less visible) changes in intimal endothelial cells that promote atherogenesis (*e.g.*, increased lipoprotein uptake, more lipoprotein oxidation, increased macrophage infiltration) (66). Additional studies will be required to assess the impact of progerin on artery wall cell function and atherogenesis. Such studies will likely add to our understanding of vascular disease in children with HGPS and further define the relevance of HGPS vascular pathology to ordinary atherosclerosis in adults within the general population.

Materials and Methods

Mice.

Zmpste24$^{-/-}$ and *Lmna*$^{G609G/G609G}$ mice have been described previously (38, 67). Sm22α-*Cre* transgenic (stock no. 017491) and mT/mG reporter (stock no. 007676) mice were purchased from The Jackson Laboratory (Bar Harbor, ME). The Sm22a-*Cre* mouse strain was genotyped by PCR with forward primer 5′-CAGACACCGAAGCTACTCTCCTTCC-3′ and reverse primer 5′-CGCATAACCAGTGAAACAGCATTGC-3′ (yielding a 500-bp product). The mT/mG mouse strain was genotyped with a mutant forward primer 5′-

TAGAGCTTGCGGAACCCTTC-3′, a wild-type forward primer 5′-AGGGAGCTGCAGTGGAGTAG-3′, and a common reverse primer 5′-CTTTAAGCCTGCCCAGAAGA-3′ (128-bp product for the mutant allele; 212-bp product for the wild-type allele). The CAG-LacZ/EGFP-KASH2 transgenic mouse (51) was genotyped with forward primer 5′-GGAGTTCGTGACCGCCGCCGGGATCACTCT-3′ and reverse primer 5′-TTTAAACGGGCCCCCTAGGTGGGAGGTGGC-3′ (yielding a ~280-bp product). Mice were housed in a specific pathogen–free barrier facility with a 12-h light/dark cycle. The mice were provided pelleted mouse chow (NIH31) and water *ad libitum* and nutritional food cups (Westbrook, ME) as required for supportive care. All animal studies were approved by UCLA's Animal Research Committee.

Cells.

Immortalized mouse aortic smooth muscle cells (#CRL-2797) were purchased from the American Type Culture Collection (Manassas, VA) and cultured in DMEM (Gibco; Gaithersburg, MD) containing 10% FBS (Hyclone), 1× nonessential amino acids (Gibco), 1 mM sodium pyruvate (Gibco), 2 mM glutamine (Gibco), and 0.2 mg/ml G418 (Gibco). The cells exhibit both synthetic and contractile phenotypes, as judged by a high proliferation rate and absence of smooth muscle myosin heavy chain expression (68), and perinuclear distribution of vimentin (69), respectively. The cells were transduced with lentivirus by UCLA's Vector Core Facility. To produce UV-treated cells, SMCs in 6-well dishes were exposed to 100mJ/cm2 UV light in a Stratalinker 2400 (Stratagene; La Jolla, CA). Cells were transfected with 100 nM *Lmnb1* siRNA (AM16706; Ambion) using RNAiMAX (Invitrogen) according to manufacturer's instructions.

pTRIPZ-Prelamin A and pTRIPZ-progerin lentiviral vectors.

A human prelamin A cDNA in pCMV-XL5 vector (#SC101048) was purchased from Origene (Rockville, MD). A human progerin cDNA was created by deleting 150 nucleotides (1818–1968) from the prelamin A cDNA with the QuikChange Lightening kit (Agilent; Santa Clara, CA) and mutagenic primers (forward primer, 5′-GCTCAGGAGCCCAGAGCCCCCAGAACTG-3′; reverse primer, 5′-CAGTTCTGGGGGCTCTGGGCTCCTGAGC-3′). The doxycycline-inducible vector pTRIPZ-hDDX5/17 (Addgene; Cambridge, MA) was digested with restriction enzymes *Age*I and *Eco*RI to delete the red fluorescence protein and shRNA sequences and then gel-purified. The human prelamin A and progerin cDNAs were amplified with the Titanium Taq PCR kit (Clontech; Mountain View, CA) and sequence-specific primers (forward primer, 5′-GTCAGATCGCACCGGATGGAGACCCCGTCCCAG-3′; and reverse primer, 5′-GTAGCCCCTTGAATTTTACATGATGCTGCAGTTCTGGGG-3′). The fragments were purified with UltraClean15 (Mo-bio) and subcloned into the prepared pTRIPZ vector with In-Fusion Cloning (Clontech). The products were amplified in XL10-Gold Ultracompetent cells (Agilent) and plasmids with the correct sequence were isolated with plasmid kits (Qiagen; Germantown, MD). Packaging of lentivirus and transduction of cells were performed by UCLA's Vector Core. Transduced cells were selected for two weeks with 1.5 μg/ml puromycin.

pLenti6-EGFP-KASH2 and pLenti6-EGFP-KASHext lentiviral vectors.

The EGFP-KASH2 sequence was amplified from pEGFP-C1-KASH2 (50) with the TaKaRa LA PCR kit (Clontech) and sequence-specific primers (forward primer, 5′-ACACCGACTCTAGAGATGGTGAGCAAGGGCGAGGA-3′; and reverse primer, 5′-GCGGGCCCTCTAGACCTAGGTGGGAGGTGGCCCGT-3′). The EGFP-KASHext sequence was amplified from pEGFP-C1-KASHext (50) with the TaKaRa LA PCR kit (Clontech) and sequence-specific primers (forward primer, 5′-ACACCGACTCTAGAGATGGTGAGCAAGGGCGAGGA-3′; and reverse primer, 5′-GCGGGCCCTCTAGACTTATCTAGATCCGGTGGATC-3′). The gel-purified fragments were subcloned into the pLenti6/v5-DEST plasmid (ThermoFisher) (linearized with *Bam*HI and *Xho*I), with In-Fusion Cloning (Clontech). The products were amplified in XL10-Gold Ultracompetent cells (Agilent) and plasmids with the correct sequences were isolated with plasmid kits (Qiagen; Germantown, MD). Packaging of lentivirus and transduction of pTRIPZ-prelamin A or pTRIPZ-progerin cells were performed by UCLA's Vector Core. Transduced cells were selected for two weeks with 2 μg/ml blasticidin.

Stretching smooth muscle cells on polydimethylsiloxane (PDMS) membranes.

Flexible PDMS membranes (1-mm-thick) were prepared in 150-mm culture dishes with the Sylgard 184 silicone elastomer kit (Dow-Corning #3097358–1004). Membranes strips (7 × 0.8 cm) were activated with a plasma cleaner, treated with 2% 3-aminopropy-triethoxysilane at RT for 45 min, washed in ethanol, and then dried at 55° C for 30 min. The membranes were incubated with 0.5 mg/ml sulfo-SANPAH in HEPES buffer and crosslinked with UV exposure (300–460 nm) for 30 sec. The washed membranes were stored at 4° C in a 100 μg/ml collagen solution (PureCol 5005; Advanced Biomatrix). Cells (1×10^5) were added to individual membrane strips in molds and incubated in media ± doxycycline for 24 h and then clamped into a custom-built stretching device. The brackets holding the membranes were attached to an L12 linear actuator (Actuonix; Victoria, Canada) controlled by a multifunction DAQ device (National Instruments; Austin, TX) and LabVIEW 2015 software (National Instruments). The membranes were stretched 6-mm at 0.5 Hz (24 h) for the cell-viability studies (trypan blue and cell protein measurements), 3-mm at 0.5 Hz (24 h) for the DNA-damage studies (western blotting studies), and 2-mm at 0.5 Hz (2 h) for the cell-damage studies (propidium iodide studies). The milder conditions for the DNA- and cell-damage studies were to examine the effects of mechanical stress prior to cell death. To measure cell protein, membranes were washed with PBS, digested with 0.1 N NaOH, and protein content measured with the D-C protein assay kit (BioRad; Richmond, CA). To stain cells with propidium iodide (PI), membranes were incubated with freshly prepared 10 μg/ml PI (ThermoFisher) and 1 μg/ml Hoechst 33342 (ThermoFisher) in Dulbecco's PBS at RT for 15-min. The stained cells were washed, fixed, and analyzed by fluorescence microscopy.

Separation of aortic adventitia and media layers.

The adventitia and media layers of the mouse aorta were separated by enzymatic digestion (44). Cleaned aortas were incubated in PBS containing 1 mg/ml collagenase type II, 1 mg/ml soybean trypsin inhibitor, and 2 mg/ml elastase (all from Worthington; Lakewood, NJ) at 37° C for 10 min. The digested aortas were placed into ice-cold PBS, cut into three

segments of equal length, and the adventitia layer unrolled from each segment. The adventitia and media (also including the endothelial cell layer) were processed immediately or frozen in liquid nitrogen for storage.

Western blotting.

Urea-soluble protein extracts from cells and tissues were prepared as described (38). Proteins were size-fractionated on 4–12% gradient polyacrylamide Bis-Tris gels (Invitrogen) and transferred to nitrocellulose membranes. The membranes were blocked with Odyssey Blocking solution (LI-COR Bioscience, Lincoln, NE) for 1 h at RT and incubated with primary antibodies at 4° C overnight. After washing the membranes with PBS containing 0.2% Tween-20, they were incubated with infrared dye (IR)–labeled secondary antibodies at RT for 1 h. The IR signals were quantified with an Odyssey infrared scanner (LI-COR Biosciences). The antibodies and concentrations are listed in Table S1.

Immunofluorescence microscopy.

Cells on coverslips or tissue sections (6–10-μm-thick) on glass slides were fixed with 4% paraformaldehyde in PBS and permeabilized with 0.2% Triton. The cells were processed for immunofluorescence microscopy as described (70, 71). The antibodies and concentrations are listed in Table S1. Confocal fluorescence microscopy images were obtained with a Zeiss LSM700 laser–scanning microscope and images along the *z*-axis were processed by Zen 2010 software (Zeiss) to generate maximum image projections. Nuclear shape abnormalities in cells were scored by two independent trained observers blinded to genotype (70, 71). A minimum of 200 cells were scored for each group.

Histological analysis.

Mice were perfused *in situ* with PBS followed by fixative solution (3% paraformaldehyde in PBS). The entire thoracic aorta was dissected free and incubated in fixative solution for 24–48 h at 4° C. Aortic rings (~2-mm-long) from the proximal ascending aorta, mid-arch, proximal descending, and mid-descending aorta were embedded in paraffin, and sections (4–6-μm) were stained with hematoxylin and eosin (HNE), Masson's trichrome, or Verhoeff-Van Gieson stain by UCLA's Translational Pathology Core Laboratory. The stained sections were coded, and photographs captured on a Nikon E600 light microscope with 20× and 40× objectives with a Nikon DS-Fi2 camera operated by NIS Elements software (Version 4.0). The images (tiff format) were imported into ImageJ1.50i, and the areas of the media and adventitia were measured. The number of nuclei in the media were counted and expressed as #nuclei/media area. Adventitial area was expressed as a percentage of total area [adventitia area/(adventitia area + media area)].

Quantitative real time-PCR.

Total RNA was isolated and treated with DNase I (Ambion, Life Technologies). RNA was reverse-transcribed with random primers, oligo(dT), and SuperScript III (Invitrogen). qPCR reactions were performed on a 7900HT Fast Real-Time PCR system (Applied Biosystems) with SYBR Green PCR Master Mix (Bioline, Taunton, MA). Transcript levels were

determined by the comparative cycle threshold method and normalized to levels of cyclophilin A. Primer sequences are listed in Table S2.

Electron microscopy.

Mice were perfused *in situ* with PBS followed by ice-cold fixative (3% paraformaldehyde in PBS). Aortic samples were incubated overnight in glutaraldehyde fixative solution containing 2.5% glutaraldehyde (EMS; Hatfield, PA), 4% paraformaldehyde (EMS), 2.1% sucrose (Sigma; Burlington, MA) and buffered with 0.1 M sodium cacodylate (Sigma). The following day, tissues were rinsed three times with 0.1 M sodium cacodylate and fixed with 2% osmium tetroxide (EMS) buffered with 0.1 M sodium cacodylate at RT for 1 h. The samples were rinsed three times with distilled water and stained overnight with 2% uranyl acetate at 4° C. The samples were rinsed three times with distilled water and dehydrated with increasing concentrations of acetone (30%, 50%, 70%, 85%, 95%, 100%; 3 × 10 min each) before infiltration with Spurr's epoxy resin (EMS) in acetone (33% for 2 h; 66% overnight; 100% for 4 h). The samples were flat-embedded in caps of BEEM capsules (EMS) and polymerized in a vacuum oven at 65° C for 24 h. The polymerized "pucks" were removed from the caps and glued onto the tops of polymerized BEEM capsules for trimming and sectioning. Sections (65-nm) were cut on a Leica UC6 ultramicrotome and picked up on freshly glow-discharged copper grids (Ted Pella; Redding, CA) that were coated with formvar and carbon. Sections on grids were then stained with Reynold's lead citrate solution for 10 min. Images were acquired with an FEI T12 transmission electron microscope set to 120 kV accelerating voltage and a Gatan 2K × 2K digital camera (Electron Imaging Center) or with a JEOL 100CX electron microscope set at 60 kV on type 4489 EM film (BRI Electron Microscopy Core Facility). Film negatives were scanned to create digital files.

Statistical analysis.

Statistical analyses were performed with Microsoft Excel for Mac 2011 and GraphPad software. Experimental groups were analyzed by a two-tailed Student's *t*-test.

Supplementary Material

Refer to Web version on PubMed Central for supplementary material.

Acknowledgments

We thank Dr. Dino Di Carlo (University of California, Los Angeles) for the use of the plasma cleaner and Ms. Lovelyn Edillo for assistance with quantification of misshapen nuclei. Virus production and transduction were performed by the IMTC/UCLA Vector Core, which is supported by CURE/P30 DK041301.

Funding: This work was supported by the National Institutes of Health (AG047192, AG035626).

References

1. DeBusk FL, The Hutchinson-Gilford progeria syndrome. Report of 4 cases and review of the literature. J. Pediatrics 80, 697–724 (1972).
2. Sarkar PK, Shinton RA, Hutchinson-Guilford progeria syndrome. Postgrad. Med. J 77, 312–317 (2001). [PubMed: 11320273]

3. Eriksson M, Brown WT, Gordon LB, Glynn MW, Singer J, Scott L, Erdos MR, Robbins CM, Moses TY, Berglund P, Dutra A, Pak E, Durkin S, Csoka AB, Boehnke M, Glover TW, Collins FS, Recurrent de novo point mutations in lamin A cause Hutchinson-Gilford progeria syndrome. Nature 423, 293–298 (2003). [PubMed: 12714972]
4. Kieran MW, Gordon L, Kleinman M, New approaches to progeria. Pediatrics 120, 834–841 (2007). [PubMed: 17908771]
5. Gordon LB, McCarten KM, Giobbie-Hurder A, Machan JT, Campbell SE, Berns SD, Kieran MW, Disease progression in Hutchinson-Gilford progeria syndrome: impact on growth and development. Pediatrics 120, 824–833 (2007). [PubMed: 17908770]
6. Merideth MA, Gordon LB, Clauss S, Sachdev V, Smith AC, Perry MB, Brewer CC, Zalewski C, Kim HJ, Solomon B, Brooks BP, Gerber LH, Turner ML, Domingo DL, Hart TC, Graf J, Reynolds JC, Gropman A, Yanovski JA, Gerhard-Herman M, Collins FS, Nabel EG, Cannon RO, 3rd, Gahl WA, Introne WJ, Phenotype and course of Hutchinson-Gilford progeria syndrome. N. Engl. J. Med 358, 592–604 (2008). [PubMed: 18256394]
7. Martin GM, Oshima J, Lessons from human progeroid syndromes. Nature 408, 263–266 (2000). [PubMed: 11089984]
8. Olive M, Harten I, Mitchell R, Beers JK, Djabali K, Cao K, Erdos MR, Blair C, Funke B, Smoot L, Gerhard-Herman M, Machan JT, Kutys R, Virmani R, Collins FS, Wight TN, Nabel EG, Gordon LB, Cardiovascular pathology in Hutchinson-Gilford progeria: correlation with the vascular pathology of aging. Arterioscler. Thromb. Vasc. Biol 30, 2301–2309 (2010). [PubMed: 20798379]
9. De Sandre-Giovannoli A, Bernard R, Cau P, Navarro C, Amiel J, Boccaccio I, Lyonnet S, Stewart CL, Munnich A, Le Merrer M, Levy N, Lamin a truncation in Hutchinson-Gilford progeria. Science 300, 2055 (2003). [PubMed: 12702809]
10. Lin F, Worman HJ, Structural organization of the human gene encoding nuclear lamin A and nuclear lamin C. J. Biol. Chem 268, 16321–16326 (1993). [PubMed: 8344919]
11. Young SG, Fong LG, Michaelis S, Prelamin A, Zmpste24, misshapen cell nuclei, and progeria--new evidence suggesting that protein farnesylation could be important for disease pathogenesis. J. Lipid Res 46, 2531–2558 (2005). [PubMed: 16207929]
12. Stuurman N, Heins S, Aebi U, Nuclear lamins: their structure, assembly, and interactions. J. Struc. Biol 122, 42–66 (1998).
13. Crisp M, Liu Q, Roux K, Rattner JB, Shanahan C, Burke B, Stahl PD, Hodzic D, Coupling of the nucleus and cytoplasm: role of the LINC complex. J. Cell Biol 172, 41–53 (2006). [PubMed: 16380439]
14. Sullivan T, Escalante-Alcalde D, Bhatt H, Anver M, Bhat N, Nagashima K, Stewart CL, Burke B, Loss of A-type lamin expression compromises nuclear envelope integrity leading to muscular dystrophy. J. Cell Biol 147, 913–920 (1999). [PubMed: 10579712]
15. Schirmer EC, Guan T, Gerace L, Involvement of the lamin rod domain in heterotypic lamin interactions important for nuclear organization. J. Cell Biol 153, 479–489 (2001). [PubMed: 11331300]
16. Goldman RD, Shumaker DK, Erdos MR, Eriksson M, Goldman AE, Gordon LB, Gruenbaum Y, Khuon S, Mendez M, Varga R, Collins FS, Accumulation of mutant lamin A causes progressive changes in nuclear architecture in Hutchinson-Gilford progeria syndrome. Proc. Natl. Acad. Sci. U. S. A 101, 8963–8968 (2004). [PubMed: 15184648]
17. Coffinier C, Chang SY, Nobumori C, Tu Y, Farber EA, Toth JI, Fong LG, Young SG, Abnormal development of the cerebral cortex and cerebellum in the setting of lamin B2 deficiency. Proc. Natl. Acad. Sci. U. S. A 107, 5076–5081 (2010). [PubMed: 20145110]
18. Chojnowski A, Ong PF, Wong ES, Lim JS, Mutalif RA, Navasankari R, Dutta B, Yang H, Liow YY, Sze SK, Boudier T, Wright GD, Colman A, Burke B, Stewart CL, Dreesen O, Progerin reduces LAP2alpha-telomere association in Hutchinson-Gilford progeria. eLife 4, (2015).
19. Hatch EM, Hetzer MW, Nuclear envelope rupture is induced by actin-based nucleus confinement. J. Cell Biol 215, 27–36 (2016). [PubMed: 27697922]
20. Denais CM, Gilbert RM, Isermann P, McGregor AL, te Lindert M, Weigelin B, Davidson PM, Friedl P, Wolf K, Lammerding J, Nuclear envelope rupture and repair during cancer cell migration. Science 352, 353–358 (2016). [PubMed: 27013428]

21. Mallampalli MP, Huyer G, Bendale P, Gelb MH, Michaelis S, Inhibiting farnesylation reverses the nuclear morphology defect in a HeLa cell model for Hutchinson-Gilford progeria syndrome. Proc. Natl. Acad. Sci. U. S. A 102, 14416–14421 (2005). [PubMed: 16186497]
22. Misteli T, Scaffidi P, Genome instability in progeria: when repair gets old. Nat. Med 11, 718–719 (2005). [PubMed: 16015360]
23. Liu B, Wang J, Chan KM, Tjia WM, Deng W, Guan X, Huang JD, Li KM, Chau PY, Chen DJ, Pei D, Pendas AM, Cadinanos J, Lopez-Otin C, Tse HF, Hutchison C, Chen J, Cao Y, Cheah KS, Tryggvason K, Zhou Z, Genomic instability in laminopathy-based premature aging. Nat. Med 11, 780–785 (2005). [PubMed: 15980864]
24. Dahl KN, Scaffidi P, Islam MF, Yodh AG, Wilson KL, Misteli T, Distinct structural and mechanical properties of the nuclear lamina in Hutchinson-Gilford progeria syndrome. Proc. Natl. Acad. Sci. U. S. A 103, 10271–10276 (2006). [PubMed: 16801550]
25. Verstraeten VL, Ji JY, Cummings KS, Lee RT, Lammerding J, Increased mechanosensitivity and nuclear stiffness in Hutchinson-Gilford progeria cells: effects of farnesyltransferase inhibitors. Aging Cell 7, 383–393 (2008). [PubMed: 18331619]
26. Scaffidi P, Misteli T, Reversal of the cellular phenotype in the premature aging disease Hutchinson-Gilford progeria syndrome. Nat. Med 11, 440–445 (2005). [PubMed: 15750600]
27. Taimen P, Pfleghaar K, Shimi T, Moller D, Ben-Harush K, Erdos MR, Adam SA, Herrmann H, Medalia O, Collins FS, Goldman AE, Goldman RD, A progeria mutation reveals functions for lamin A in nuclear assembly, architecture, and chromosome organization. Proc. Natl. Acad. Sci. U. S. A 106, 20788–20793 (2009). [PubMed: 19926845]
28. Liu GH, Barkho BZ, Ruiz S, Diep D, Qu J, Yang SL, Panopoulos AD, Suzuki K, Kurian L, Walsh C, Thompson J, Boue S, Fung HL, Sancho-Martinez I, Zhang K, Yates J, 3rd, Izpisua Belmonte JC, Recapitulation of premature ageing with iPSCs from Hutchinson-Gilford progeria syndrome. Nature 472, 221–225 (2011). [PubMed: 21346760]
29. Toth JI, Yang SH, Qiao X, Beigneux AP, Gelb MH, Moulson CL, Miner JH, Young SG, Fong LG, Blocking protein farnesyltransferase improves nuclear shape in fibroblasts from humans with progeroid syndromes. Proc. Natl. Acad. Sci. U. S. A 102, 12873–12878 (2005). [PubMed: 16129834]
30. Glynn MW, Glover TW, Incomplete processing of mutant lamin A in Hutchinson-Gilford progeria leads to nuclear abnormalities, which are reversed by farnesyltransferase inhibition. Hum. Mol. Genet 14, 2959–2969 (2005). [PubMed: 16126733]
31. Capell BC, Erdos MR, Madigan JP, Fiordalisi JJ, Varga R, Conneely KN, Gordon LB, Der CJ, Cox AD, Collins FS, Inhibiting farnesylation of progerin prevents the characteristic nuclear blebbing of Hutchinson-Gilford progeria syndrome. Proc. Natl. Acad. Sci. U. S. A 102, 12879–12884 (2005). [PubMed: 16129833]
32. Yang SH, Meta M, Qiao X, Frost D, Bauch J, Coffinier C, Majumdar S, Bergo MO, Young SG, Fong LG, A farnesyltransferase inhibitor improves disease phenotypes in mice with a Hutchinson-Gilford progeria syndrome mutation. J. Clin. Invest 116, 2115–2121 (2006). [PubMed: 16862216]
33. Sagelius H, Rosengardten Y, Hanif M, Erdos MR, Rozell B, Collins FS, Eriksson M, Targeted transgenic expression of the mutation causing Hutchinson-Gilford progeria syndrome leads to proliferative and degenerative epidermal disease. J. Cell Sci 121, 969–978 (2008). [PubMed: 18334552]
34. Wang Y, Panteleyev AA, Owens DM, Djabali K, Stewart CL, Worman HJ, Epidermal expression of the truncated prelamin A causing Hutchinson-Gilford progeria syndrome: effects on keratinocytes, hair and skin. Hum. Mol. Genet 17, 2357–2369 (2008). [PubMed: 18442998]
35. Osorio FG, Navarro CL, Cadinanos J, Lopez-Mejia IC, Quiros PM, Bartoli C, Rivera J, Tazi J, Guzman G, Varela I, Depetris D, de Carlos F, Cobo J, Andres V, De Sandre-Giovannoli A, Freije JM, Levy N, Lopez-Otin C, Splicing-directed therapy in a new mouse model of human accelerated aging. Sci. Transl. Med 3, 106ra107 (2011).
36. Schmidt E, Nilsson O, Koskela A, Tuukkanen J, Ohlsson C, Rozell B, Eriksson M, Expression of the Hutchinson-Gilford progeria mutation during osteoblast development results in loss of osteocytes, irregular mineralization, and poor biomechanical properties. J. Biol. Chem 287, 33512–33522 (2012). [PubMed: 22893709]

37. Baek JH, Schmidt E, Viceconte N, Strandgren C, Pernold K, Richard TJ, Van Leeuwen FW, Dantuma NP, Damberg P, Hultenby K, Ulfhake B, Mugnaini E, Rozell B, Eriksson M, Expression of progerin in aging mouse brains reveals structural nuclear abnormalities without detectible significant alterations in gene expression, hippocampal stem cells or behavior. Hum. Mol. Genet 24, 1305–1321 (2015). [PubMed: 25343989]
38. Lee JM, Nobumori C, Tu Y, Choi C, Yang SH, Jung HJ, Vickers TA, Rigo F, Bennett CF, Young SG, Fong LG, Modulation of LMNA splicing as a strategy to treat prelamin A diseases. J. Clin. Invest 126, 1592–1602 (2016). [PubMed: 26999604]
39. Varga R, Eriksson M, Erdos MR, Olive M, Harten I, Kolodgie F, Capell BC, Cheng J, Faddah D, Perkins S, Avallone H, San H, Qu X, Ganesh S, Gordon LB, Virmani R, Wight TN, Nabel EG, Collins FS, Progressive vascular smooth muscle cell defects in a mouse model of Hutchinson-Gilford progeria syndrome. Proc. Natl. Acad. Sci. U. S. A 103, 3250–3255 (2006). [PubMed: 16492728]
40. Stehbens WE, Wakefield SJ, Gilbert-Barness E, Olson RE, Ackerman J, Histological and ultrastructural features of atherosclerosis in progeria. Cardiovasc. Path 8, 29–39 (1999). [PubMed: 10722246]
41. Stehbens WE, Delahunt B, Shozawa T, Gilbert-Barness E, Smooth muscle cell depletion and collagen types in progeric arteries. Cardiovasc. Path 10, 133–136 (2001). [PubMed: 11485857]
42. Song M, San H, Anderson SA, Cannon RO, 3rd, Orlic D, Shear stress-induced mechanotransduction protein deregulation and vasculopathy in a mouse model of progeria. Stem Cell Res. Therap 5, 41 (2014). [PubMed: 24661531]
43. Klionsky DJ, Eskelinen EL, Deretic V, Autophagosomes, phagosomes, autolysosomes, phagolysosomes, autophagolysosomes... wait, I'm confused. Autophagy 10, 549–551 (2014). [PubMed: 24657946]
44. Geisterfer AA, Peach MJ, Owens GK, Angiotensin II induces hypertrophy, not hyperplasia, of cultured rat aortic smooth muscle cells. Circ. Res 62, 749–756 (1988). [PubMed: 3280155]
45. Jung HJ, Tu Y, Yang SH, Tatar A, Nobumori C, Wu D, Young SG, Fong LG, New Lmna knock-in mice provide a molecular mechanism for the 'segmental aging' in Hutchinson-Gilford progeria syndrome. Hum. Mol. Genet 23, 1506–1515 (2014). [PubMed: 24203701]
46. Chiu JJ, Chien S, Effects of disturbed flow on vascular endothelium: pathophysiological basis and clinical perspectives. Physiol. Rev 91, 327–387 (2011). [PubMed: 21248169]
47. Assemat P, Siu KK, Armitage JA, Hokke SN, Dart A, Chin-Dusting J, Hourigan K, Haemodynamical stress in mouse aortic arch with atherosclerotic plaques: Preliminary study of plaque progression. Comput. Struc. Biotech. J 10, 98–106 (2014).
48. Chen CY, Chi YH, Mutalif RA, Starost MF, Myers TG, Anderson SA, Stewart CL, Jeang KT, Accumulation of the inner nuclear envelope protein Sun1 is pathogenic in progeric and dystrophic laminopathies. Cell 149, 565–577 (2012). [PubMed: 22541428]
49. Haque F, Lloyd DJ, Smallwood DT, Dent CL, Shanahan CM, Fry AM, Trembath RC, Shackleton S, SUN1 interacts with nuclear lamin A and cytoplasmic nesprins to provide a physical connection between the nuclear lamina and the cytoskeleton. Mol. Cell Biol 26, 3738–3751 (2006). [PubMed: 16648470]
50. Stewart-Hutchinson PJ, Hale CM, Wirtz D, Hodzic D, Structural requirements for the assembly of LINC complexes and their function in cellular mechanical stiffness. Exp. Cell Res 314, 1892–1905 (2008). [PubMed: 18396275]
51. Razafsky D, Potter C, Hodzic D, Validation of a Mouse Model to Disrupt LINC Complexes in a Cell-specific Manner. JoVE, e53318 (2015). [PubMed: 26710083]
52. Holtwick R, Gotthardt M, Skryabin B, Steinmetz M, Potthast R, Zetsche B, Hammer RE, Herz J, Kuhn M, Smooth muscle-selective deletion of guanylyl cyclase-A prevents the acute but not chronic effects of ANP on blood pressure. Proc. Natl. Acad. Sci. U. S. A 99, 7142–7147 (2002). [PubMed: 11997476]
53. Muzumdar MD, Tasic B, Miyamichi K, Li L, Luo L, A global double-fluorescent Cre reporter mouse. Genesis 45, 593–605 (2007). [PubMed: 17868096]

54. Gordon LB, Harten IA, Patti ME, Lichtenstein AH, Reduced adiponectin and HDL cholesterol without elevated C-reactive protein: clues to the biology of premature atherosclerosis in Hutchinson-Gilford Progeria Syndrome. J. Pediatrics 146, 336–341 (2005).

55. Hennekam RC, Hutchinson-Gilford progeria syndrome: review of the phenotype. Amer. J. Med. Genet 140, 2603–2624 (2006). [PubMed: 16838330]

56. Moulson CL, Fong LG, Gardner JM, Farber EA, Go G, Passariello A, Grange DK, Young SG, Miner JH, Increased progerin expression associated with unusual LMNA mutations causes severe progeroid syndromes. Hum. Mut 28, 882–889 (2007). [PubMed: 17469202]

57. Turlo KA, Scapa J, Bagher P, Jones AW, Feil R, Korthuis RJ, Segal SS, Iruela-Arispe ML, beta1-integrin is essential for vasoregulation and smooth muscle survival in vivo. Arterioscler. Thromb. Vasc. Biol 33, 2325–2335 (2013). [PubMed: 23887637]

58. Sibinga NE, Foster LC, Hsieh CM, Perrella MA, Lee WS, Endege WO, Sage EH, Lee ME, Haber E, Collagen VIII is expressed by vascular smooth muscle cells in response to vascular injury. Circ. Res 80, 532–541 (1997). [PubMed: 9118484]

59. Lopes J, Adiguzel E, Gu S, Liu SL, Hou G, Heximer S, Assoian RK, Bendeck MP, Type VIII collagen mediates vessel wall remodeling after arterial injury and fibrous cap formation in atherosclerosis. Amer. J. Path 182, 2241–2253 (2013). [PubMed: 23567639]

60. Shin JW, Spinler KR, Swift J, Chasis JA, Mohandas N, Discher DE, Lamins regulate cell trafficking and lineage maturation of adult human hematopoietic cells. Proc. Natl. Acad. Sci. U. S. A 110, 18892–18897 (2013). [PubMed: 24191023]

61. Shimi T, Butin-Israeli V, Adam SA, Hamanaka RB, Goldman AE, Lucas CA, Shumaker DK, Kosak ST, Chandel NS, Goldman RD, The role of nuclear lamin B1 in cell proliferation and senescence. Genes Dev 25, 2579–2593 (2011). [PubMed: 22155925]

62. Broers JL, Peeters EA, Kuijpers HJ, Endert J, Bouten CV, Oomens CW, Baaijens FP, Ramaekers FC, Decreased mechanical stiffness in LMNA−/− cells is caused by defective nucleo-cytoskeletal integrity: implications for the development of laminopathies. Hum. Mol. Genet 13, 2567–2580 (2004). [PubMed: 15367494]

63. Raab M, Gentili M, de Belly H, Thiam HR, Vargas P, Jimenez AJ, Lautenschlaeger F, Voituriez R, Lennon-Dumenil AM, Manel N, Piel M, ESCRT III repairs nuclear envelope ruptures during cell migration to limit DNA damage and cell death. Science 352, 359–362 (2016). [PubMed: 27013426]

64. Jevtic P, Edens LJ, Li X, Nguyen T, Chen P, Levy DL, Concentration-dependent Effects of Nuclear Lamins on Nuclear Size in Xenopus and Mammalian Cells. J. Biol. Chem 290, 27557–27571 (2015). [PubMed: 26429910]

65. Clarke MC, Figg N, Maguire JJ, Davenport AP, Goddard M, Littlewood TD, Bennett MR, Apoptosis of vascular smooth muscle cells induces features of plaque vulnerability in atherosclerosis. Nat. Med 12, 1075–1080 (2006). [PubMed: 16892061]

66. Lusis AJ, Atherosclerosis. Nature 407, 233–241 (2000). [PubMed: 11001066]

67. Bergo MO, Gavino B, Ross J, Schmidt WK, Hong C, Kendall LV, Mohr A, Meta M, Genant H, Jiang Y, Wisner ER, Van Bruggen N, Carano RA, Michaelis S, Griffey SM, Young SG, Zmpste24 deficiency in mice causes spontaneous bone fractures, muscle weakness, and a prelamin A processing defect. Proc. Natl. Acad. Sci. U. S. A 99, 13049–13054 (2002). [PubMed: 12235369]

68. Rensen SS, Doevendans PA, van Eys GJ, Regulation and characteristics of vascular smooth muscle cell phenotypic diversity. Neth. Heart J 15, 100–108 (2007). [PubMed: 17612668]

69. Worth NF, Rolfe BE, Song J, Campbell GR, Vascular smooth muscle cell phenotypic modulation in culture is associated with reorganisation of contractile and cytoskeletal proteins. Cell Motility Cytoskel 49, 130–145 (2001). [PubMed: 11668582]

70. Fong LG, Ng JK, Meta M, Cote N, Yang SH, Stewart CL, Sullivan T, Burghardt A, Majumdar S, Reue K, Bergo MO, Young SG, Heterozygosity for Lmna deficiency eliminates the progeria-like phenotypes in Zmpste24-deficient mice. Proc. Natl. Acad. Sci. U. S. A 101, 18111–18116 (2004). [PubMed: 15608054]

71. Fong LG, Ng JK, Lammerding J, Vickers TA, Meta M, Cote N, Gavino B, Qiao X, Chang SY, Young SR, Yang SH, Stewart CL, Lee RT, Bennett CF, Bergo MO, Young SG, Prelamin A and

lamin A appear to be dispensable in the nuclear lamina. J. Clin. Invest 116, 743–752 (2006). [PubMed: 16511604]

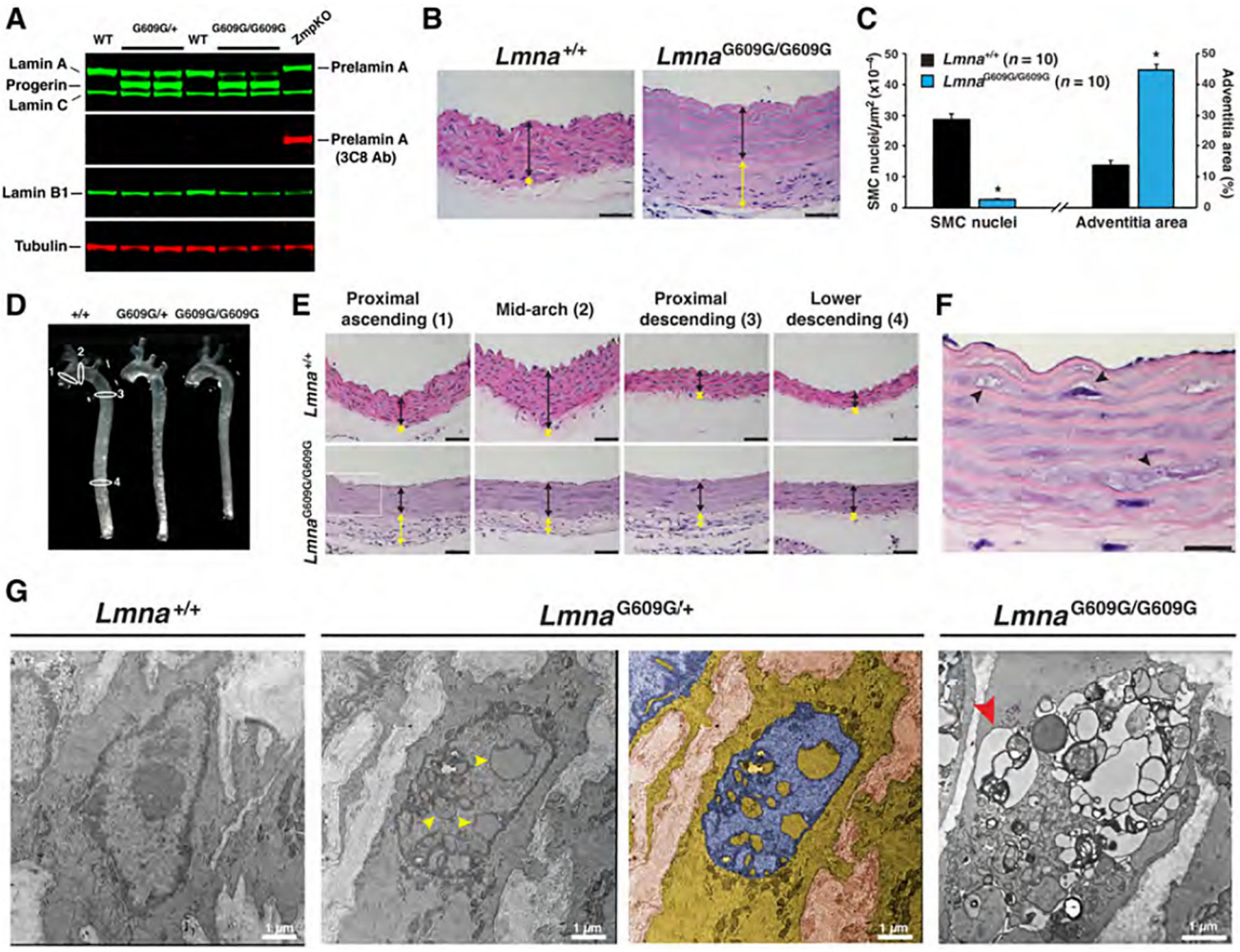

Figure 1. Mice expressing progerin develop aortic pathology.

Mouse aortas analyzed by western blotting, histology, and electron microscopy. (a) Western blot showing the synthesis of progerin but not prelamin A in aortas from *Lmna*$^{G609G/+}$ (G609G/+) and *Lmna*$^{G609G/G609G}$ (G609G/G609G) mice. Average progerin levels (relative to tubulin) were 1.15 and 1.43 for heterozygous and homozygous G609G mice, respectively. (b) Representative hematoxylin and eosin (HNE)–stained sections of the ascending aorta from a 4-month-old *Lmna*$^{+/+}$ and *Lmna*$^{G609G/G609G}$ mouse. Colored lines identify the aortic media (black) and adventitia (yellow). Scale bar, 50 μm. (c) Bar graph showing fewer smooth muscle cell (SMC) nuclei (left) and greater adventitial area (right) in the ascending aorta (inner curvature) of 4-month-old *Lmna*$^{G609G/G609G}$ mice (blue), compared with age-matched wild-type mice (black). Mean ± SEM; $n = 10$/group. *Lmna*$^{G609G/G609G}$ *vs.* wild-type; $*p < 0.001$. (d) Thoracic aortas from wild-type (+/+), *Lmna*$^{G609G/+}$ (G609G/+), and *Lmna*$^{G609G/G609G}$ (G609G/G609G) mice. Numbered white ovals identify locations for sections in panel e. (e) HNE-stained sections of four regions of the thoracic aorta from 4-month-old *Lmna*$^{+/+}$ and *Lmna*$^{G609G/G609G}$ mice. Colored lines identify the adventitia (yellow) and media (black). Scale bar, 40 μm. (f) Enlarged image of the proximal ascending aorta (boxed area in panel e) showing vacuolated SMCs (black arrowheads). Scale bar, 20 μm. (g) Electron micrographs showing SMC nuclei in *Lmna*$^{+/+}$, *Lmna*$^{G609G/+}$, and

Lmna$^{G609G/G609G}$ mice. Yellow arrowheads point to intranuclear vesicles in *Lmna*$^{G609G/+}$ aortas. A duplicate image is colorized to show the nucleoplasm (blue) and cytoplasm (yellow). Red arrowhead points to a cytoplasmic vacuole in a *Lmna*$^{G609G/G609G}$ aortic SMC.

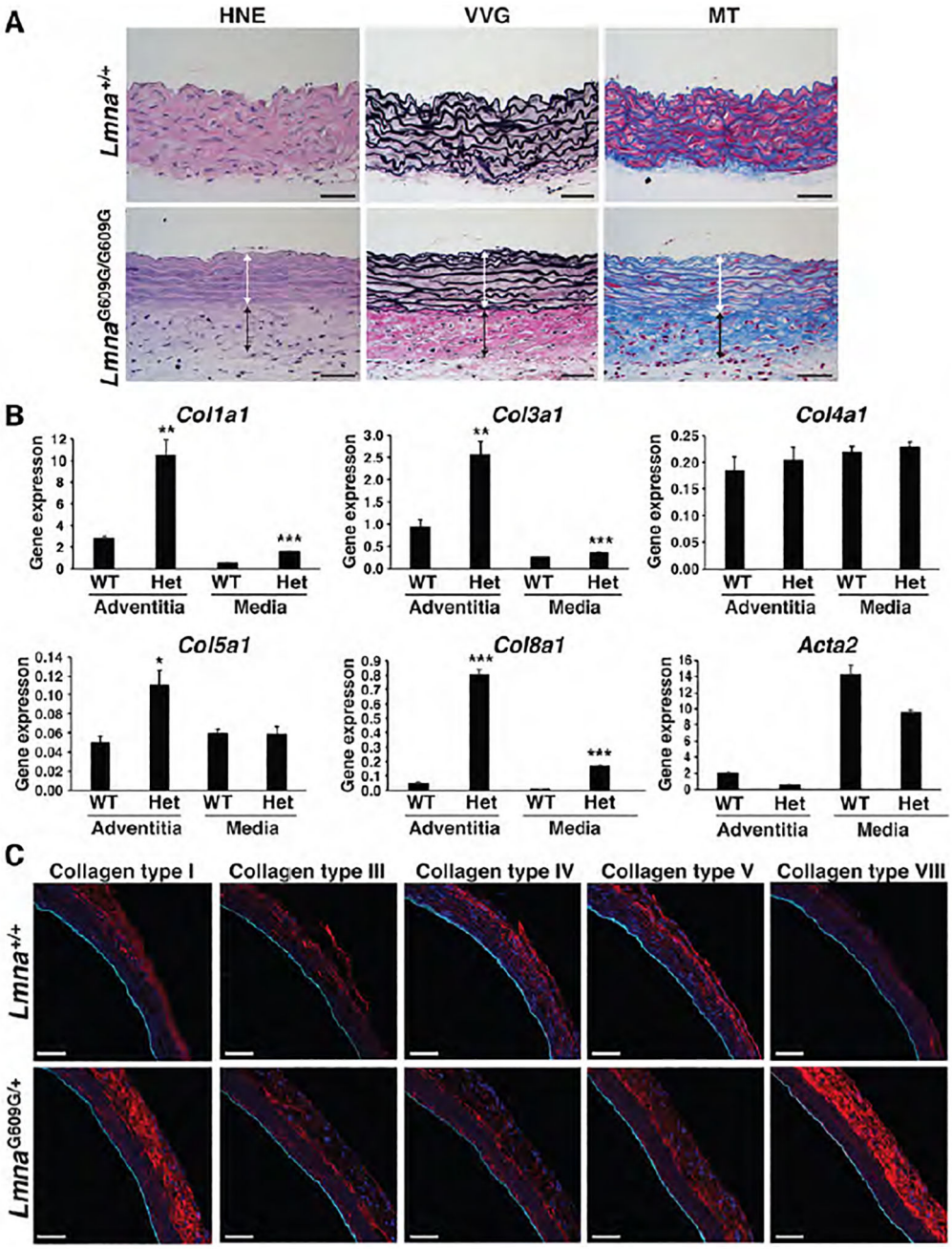

Figure 2. Collagen synthesis is increased in the adventitia of *Lmna*^{G609G} mice.

Collagen synthesis in the aorta of *Lmna*$^{+/+}$ and *Lmna*^{G609G} mice was examined by histochemistry, gene-expression studies, and immunofluorescence microscopy. (a) Histochemical studies show that collagen content is increased in the adventitia of a 4-month-old *Lmna*$^{G609G/G609G}$ mouse. HNE: blue, nuclei; pink, cytoplasm. Verhoeff-Van Gieson (VVG) stain: black, elastic fibers and nuclei; red, collagen. Masson's trichrome (MT) stain: pink/red, cytoplasm; blue, collagen. Colored lines identify the media (white) and adventitial (black) layers. Scale bar, 50 μm. (b) RT-PCR studies showing that *Col1a1* and *Col8a1* expression are increased in the adventitia of 12-month-old *Lmna*$^{G609G/+}$ mice (mean ±

SEM; $n = 3$). *Lmna*$^{G609G/+}$ *vs.* wild-type; *$p < 0.05$, **$p < 0.01$, ***$p < 0.001$. (c) Serial frozen sections of the ascending aorta from 12-month-old wild-type and *Lmna*$^{G609G/+}$ mice were stained with antibodies against collagen types I, III, IV, V, and VIII (red) and CD31 (cyan) and examined by confocal fluorescence microscopy. Scale bar, 50 μm.

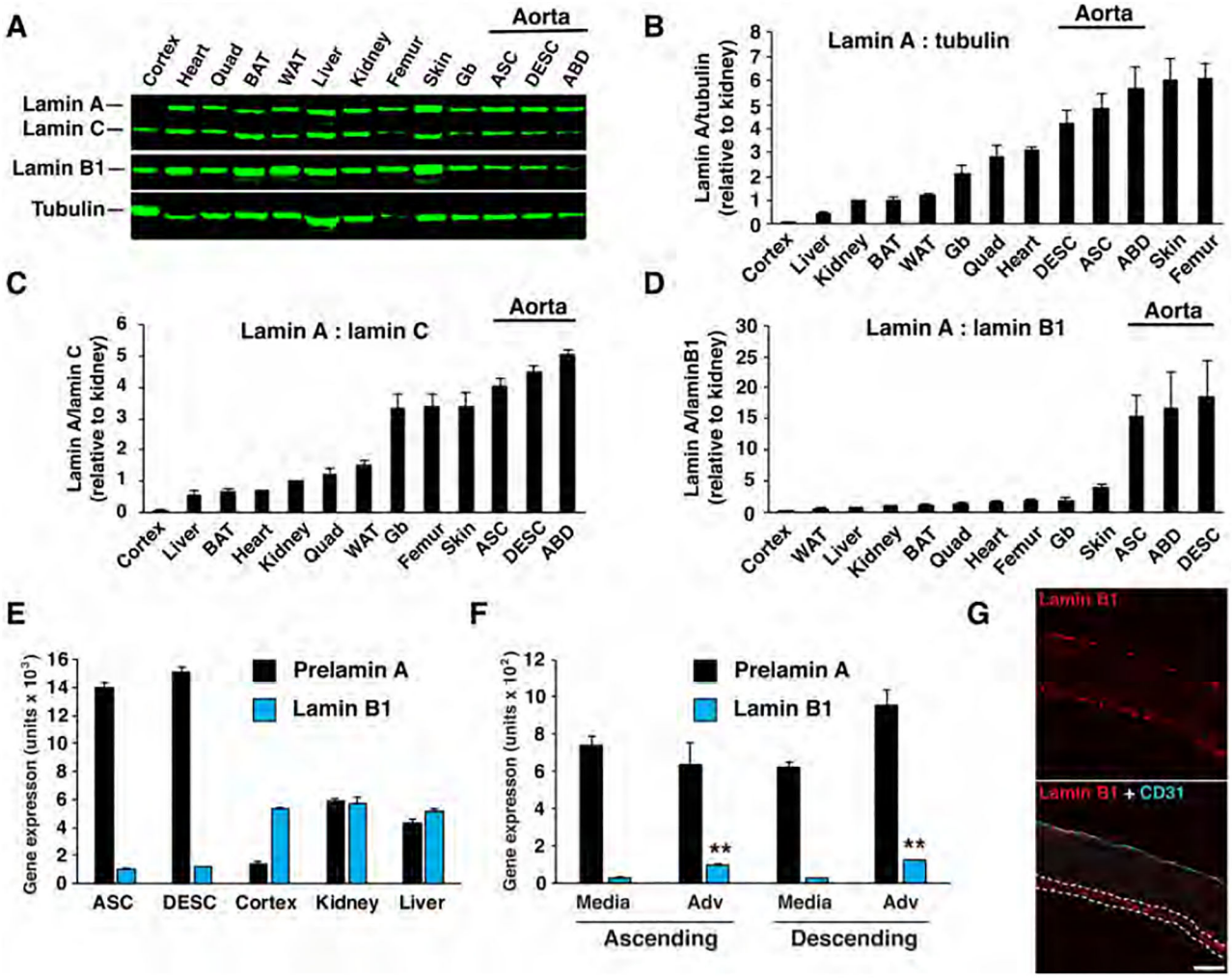

Figure 3. Lamin A is expressed at high levels in the aorta of wild-type mice.

Nuclear lamin expression in different tissues of wild-type mice was measured by western blotting, RT-PCR, and fluorescence microscopy. (a) Representative western blot comparing lamin A, lamin C, and lamin B1 levels in different tissues. Tubulin was measured as a loading control. Cortex, cerebral cortex; BAT, brown adipose tissue; WAT, white adipose tissue; Gb, gallbladder; ASC, ascending aorta; DESC, descending aorta; ABD, abdominal aorta. Graphs showing lamin A expression relative to tubulin (b), relative to lamin C (c), and relative to lamin B1 (d). For panels b–d, the tissues are arranged in ascending order from left to right, with the expression in kidney set at a value of one (mean ± SEM; $n = 4$ mice). (e) RT-PCR studies comparing the expression of prelamin A (black) and *Lmnb1* (blue) in tissues (mean ± SEM; $n = 4$ mice). (f) RT-PCR studies comparing the expression of prelamin A (black) and *Lmnb1* (blue) in the media and adventitia (Adv) layers of wild-type mice (mean ± SEM; $n = 4$ mice). Media *vs.* adventitia; $^{**}p < 0.001$. (g) Confocal fluorescence microscopy images showing the expression of CD31 (cyan) and lamin B1 (red) in the ascending aorta of a wild-type mouse. In the merged image, the adventitia is outlined by dotted white lines (see Fig. S4g). Scale bar, 50 μm.

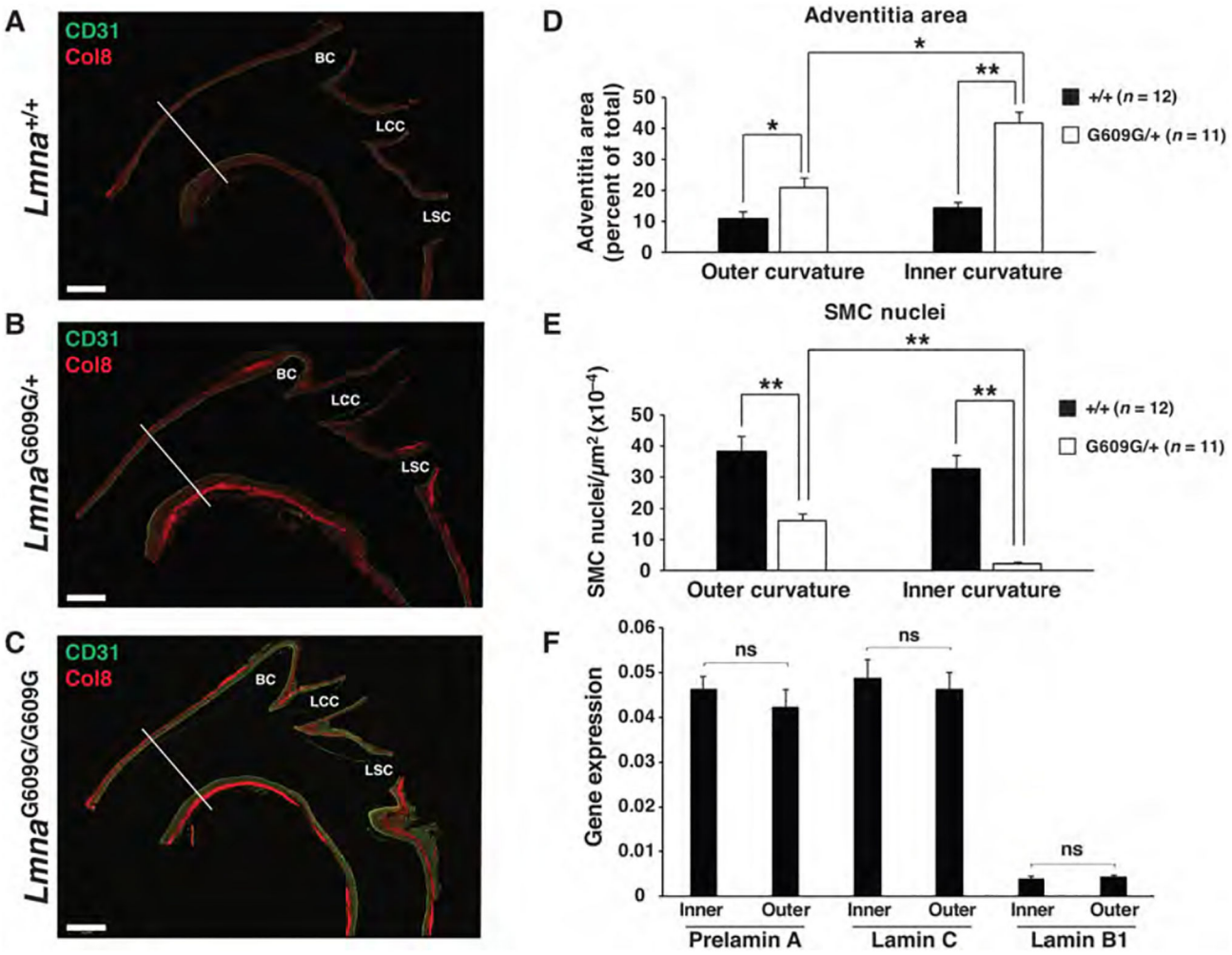

Figure 4. Vascular pathology is more severe along the inner curvature of the ascending aorta and branches of the aortic arch.

The number of SMC nuclei and adventitial area were quantified at the inner and outer curvature of the ascending thoracic aorta of *Lmna*^{G609G} mice. The white lines in panels a–c identify the location where the measurements were made. (a–c) Composite fluorescence microscopy images of the ascending aorta stained with antibodies against CD31 (green) and collagen type VIII (red) in 12-month-old *Lmna*$^{+/+}$ and *Lmna*$^{G609G/+}$ mice, and a 4-month-old *Lmna*$^{G609G/G609G}$ mouse. BC, brachiocephalic; LCC, left common carotid; and LSC, left subclavian. Scale bar, 500 μm. (d) Bar graph showing adventitial area (as a percentage of total area) in wild-type (black bars) and *Lmna*$^{G609G/+}$ (white bars) mice at the outer and inner curvature of the ascending aorta. (e) Bar graph showing the number of SMC nuclei (relative to media area) in wild-type (black bars) and *Lmna*$^{G609G/+}$ (white bars) mice at the outer and inner curvature of the ascending aorta. Mean ± SEM for wild-type ($n = 12$) and *Lmna*$^{G609G/+}$ ($n = 11$) mice; *$p < 0.02$ and **$p < 0.001$. (f) RT-PCR studies measuring prelamin A, lamin C, and *Lmnb1* expression at the inner and outer curvature in wild-type mice (mean ± SEM; $n = 4$). Inner *vs.* outer; ns (nonsignificant), $p > 0.20$.

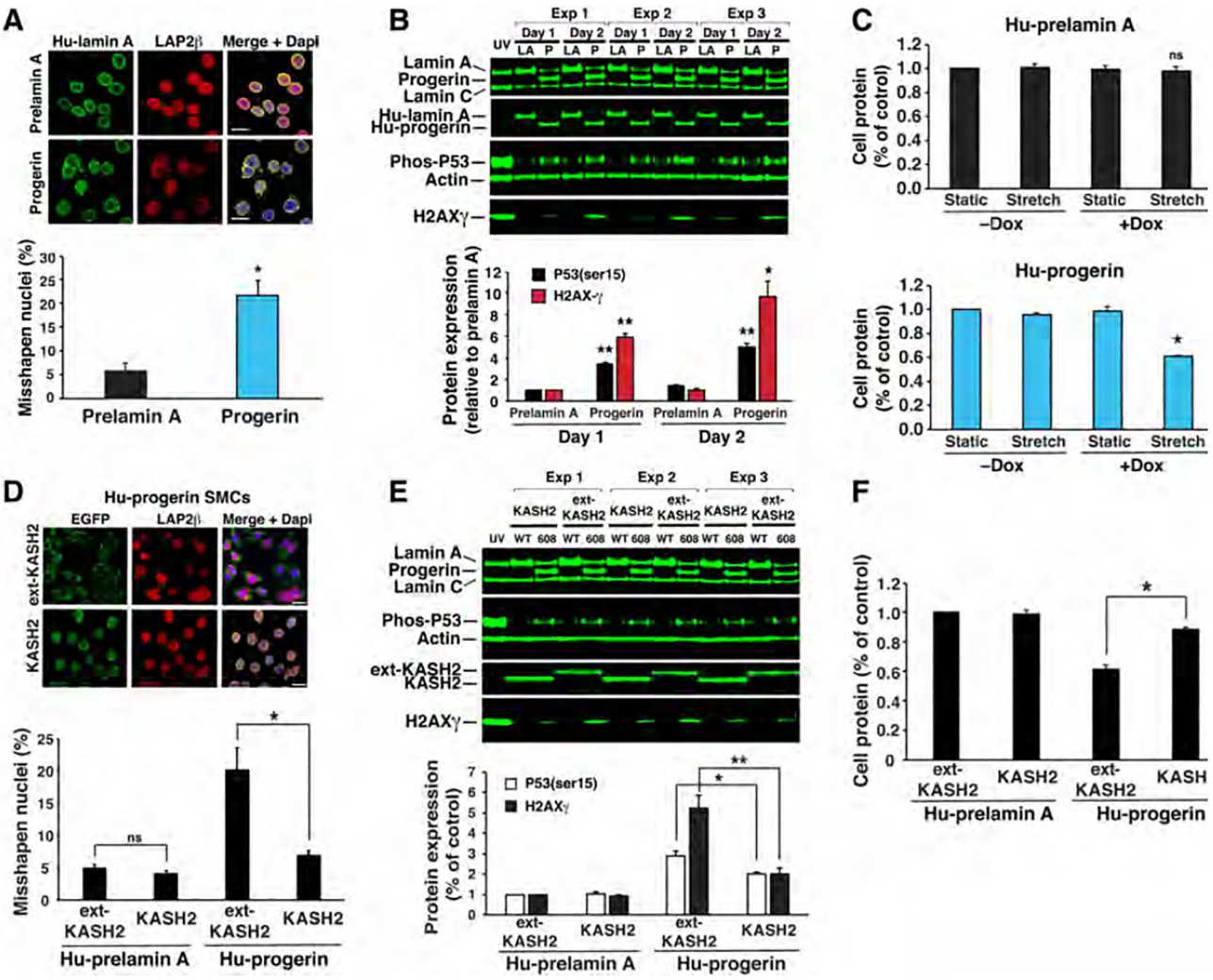

Figure 5. Disrupting the LINC complex in SMCs ameliorates phenotypes elicited by progerin.

(a) Microscopy images showing progerin increases misshapen nuclei in SMCs. Scale bar, 20 μm. Bar graph shows quantification of misshapen nuclei (mean ± SEM; $n = 3$ experiments). *$p < 0.02$. (b) Western blots showing that progerin (P) induces P53 phosphorylation and H2AX-γ expression compared to lamin A (LA). Cells exposed to UV light were included as a control. The bar graph shows the expression of P53 phosphorylation (black) and H2AX-γ (red) after 1- or 2-days (mean ± SEM; $n = 3$ experiments). Progerin *vs.* prelamin A; *$p <$ 0.01, **$p < 0.001$. (c) Uniaxial strain induces cell death in progerin-expressing SMCs. Prelamin A- and progerin-expressing cells were exposed to stretching (6 mm, 0.5 Hz) or static conditions for 1 day. Cell protein was measured and expressed relative to static cells (mean ± SEM; $n = 3$ experiments). Stretch *vs.* static; *$p < 0.001$. (d) Microscopy images showing that KASH2 reduces misshapen nuclei in progerin-expressing cells as compared to ext-KASH2. Scale bar, 20 μm. Bar graph shows quantification of misshapen nuclei (mean ± SEM; $n = 3$ experiments). KASH2 *vs.* ext-KASH2; *$p < 0.02$. (e) Western blot showing that KASH2 reduces H2AX-γ levels and p53 phosphorylation in unstrained, progerin-expressing cells. The bar graph shows the average expression of P53 phosphorylation (white) and

H2AX-g (black) after 1 day (mean ± SEM; $n = 3$ experiments). KASH2 *vs.* ext-KASH2; *$p < 0.05$, **$p < 0.01$. (f) KASH2 reduces cell death in stretched, progerin-expressing cells. The bar graph shows cell protein levels relative to stretched, prelamin A/ext-KASH2–expressing cells (mean ± SEM; $n = 3$ experiments). KASH2 *vs.* ext-KASH2; *$p < 0.001$.

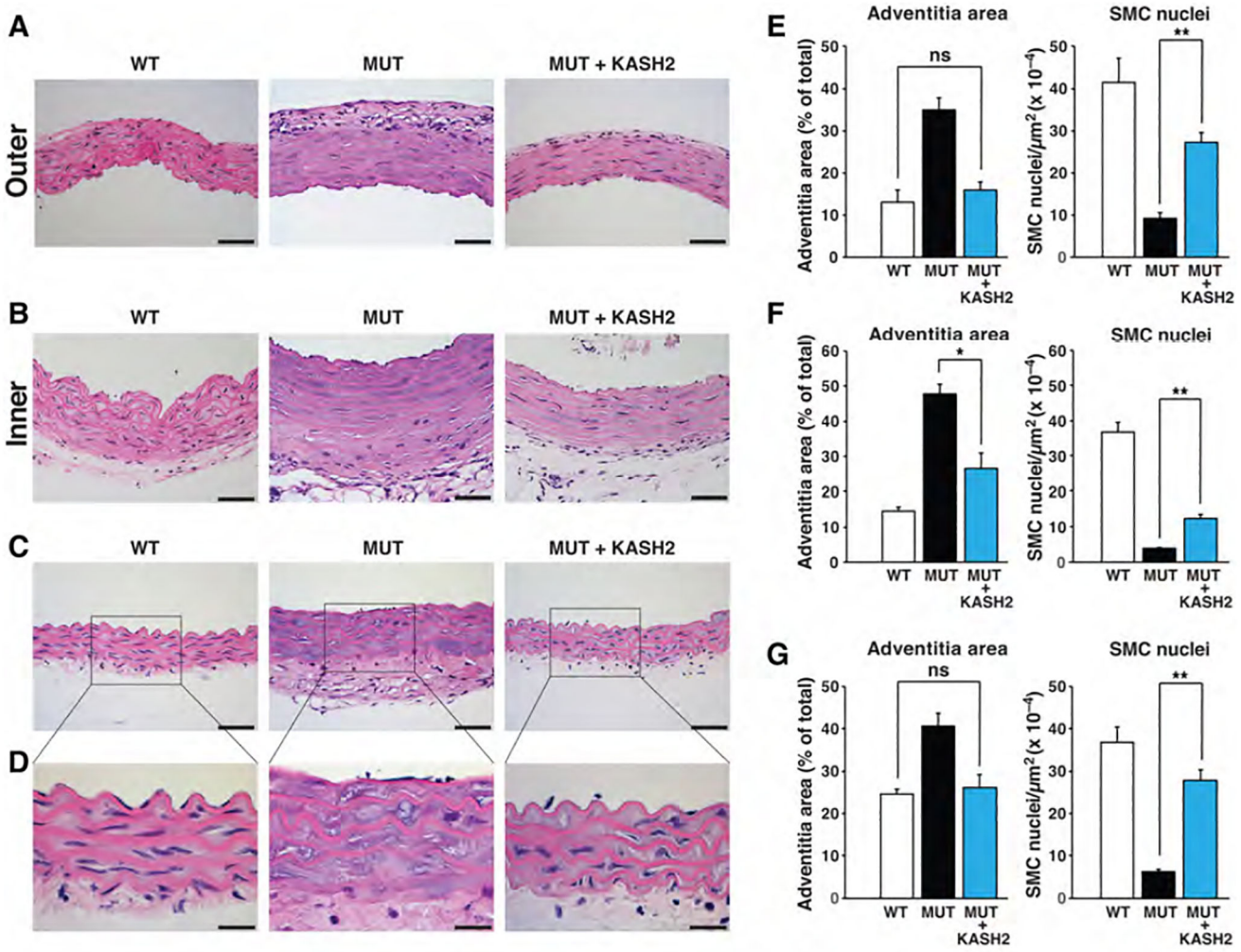

Figure 6. The expression of the KASH2 domain in smooth muscle cells ameliorates aortic disease in *Lmna*$^{G609G/G609G}$ mice.

The *Cre*-conditional KASH2–EGFP transgene was bred into *Lmna*$^{G609G/G609G}$ mice harboring the SMC-specific *Sm22–Cre* transgene. Three groups were examined: WT, *Lmna*$^{+/+}$KASH2–EGFP^{+} *Sm22-Cre*$^{+}$; MUT, *Lmna*$^{G609G/G609G}$KASH2–EGFP^{+} *Sm22-Cre*$^{-}$; and MUT + KASH2, *Lmna*$^{G609G/G609G}$KASH2–EGFP^{+} *Sm22-Cre*$^{+}$. Adventitial fibrosis and SMC nuclei were quantified in the three groups. (a–d) Representative photographs of HNE-stained cross sections at the outer (a) and inner curvature (b) of the ascending aorta, and proximal descending aorta (c–d). Scale bars, 50 μm for panels a–c; 20 μm for panel d. (e) Adventitial area (as a percent of total area) and numbers of SMC nuclei (per media area) at the outer ascending thoracic aorta (mean ± SEM; $n = 6$/group). (f) Adventitial area and numbers of SMC nuclei at the inner ascending thoracic aorta (mean ± SEM; $n = 6$/group). (g) Adventitial area and numbers of SMC nuclei in the proximal descending thoracic aorta (mean ± SEM; $n = 6$/group). *$p < 0.01$; **$p < 0.001$; ns, nonsignificant defined as $p > 0.40$.